p-ISSN 3030-4830

VELOCITY-DEPENDENT DEFORMATION MECHANISM OF FeNiCrCoTi HIGH-ENTROPY ALLOY UNDER VIBRATION-ASSISTED MACHINING

Trong-Tung Dam[1], Thi-Quy Vu[2], Xuan-Truong Vu[2], Dinh-Quan Doan[2,*]

[1] *Solutions and Services Provides Joint Stock Company, Ha Noi*

[2] *Hung Yen University of Technology and Education*

* *Corresponding author: dinhquandoan@gmail.com*

Received: 29/09/2025
Revised: 18/11/2025
Accepted for publication: 12/12/2025

Abstract:

Vibration-assisted machining has shown great potential for improving the processing of hard and tough materials, but its mechanisms in high-entropy alloys (HEAs) remain unclear. In this study, molecular dynamics simulations are employed to investigate the velocity-dependent behavior of FeNiCrCoTi monocrystal during vibration-assisted nano-machining. The study examines machining forces, shear strain, von Mises stress, dislocation evolution, temperature distribution, and surface morphology. The results reveal that higher velocities increase normal and tangential forces, stress concentration, and local temperature, while reducing shear strain, dislocation accumulation, groove width, and worn atom number. These findings provide new atomistic insights into the deformation and material removal mechanisms of HEAs under vibration-assisted machining.

Keywords: *vibration-assisted machining, MD simulation, velocity, high-entropy alloy.*

1. Introduction

High-entropy alloys (HEAs) consist of multiple principal elements in near-equiatomic ratios [1]. Their high configurational entropy promotes the formation of simple solid solutions instead of complex intermetallic phases, leading to exceptional properties such as high strength, hardness, corrosion resistance, and thermal stability [2]. These advantages make HEAs promising for advanced structural and functional applications in aerospace, turbines, and nuclear systems [3]. Recent studies have shown that adding Ti to FeNiCrCo alloys significantly enhances strength, wear resistance, and thermal stability, enabling FeNiCrCoTi HEA alloys to withstand extreme mechanical and thermal loads. Studies have reported high hardness, improved oxidation resistance, and stable strain behavior in FeNiCrCoTi-based alloys. Therefore, FeNiCrCoTi exhibits strong potential as a structural and protective coating material for harsh operating environments [4, 5].

Vibration-assisted machining has emerged as an effective technique for processing hard and tough materials [6]. By applying controlled vibration, vibration-assisted machining reduces cutting forces, improves surface finish, suppresses crack propagation, and enhances material removal compared with conventional machining [7]. Although some studies have explored the machinability of HEA alloys, the deformation mechanism of FeNiCrCoTi under vibration has not been thoroughly investigated. The effect of machining velocity has rarely been clarified, even though velocity strongly governs atomic motion, defect generation, and energy dissipation. Experimental investigations face challenges due to cost, technological limitations, and difficulties in probing atomistic details.

Molecular dynamics (MD) simulation provides a powerful means to analyze machining at the atomic scale [8, 9]. Previous MD studies have offered valuable insights into chip formation, distribution of stress and temperature, and dislocation dynamics under vibration-assisted

conditions. However, most of these efforts have focused on ceramics or single-component metals, leaving HEAs relatively unexplored. Specifically, the velocity-dependent behavior of FeNiCrCoTi during vibration-assisted machining has not yet been systematically investigated. In this study, MD simulations are performed to examine vibration-assisted nano-scratching of FeNiCrCoTi alloy at different velocities under fixed vibration conditions. The results provide new atomistic insights into the velocity-dependent deformation and material removal mechanisms of HEAs.

2. Methods

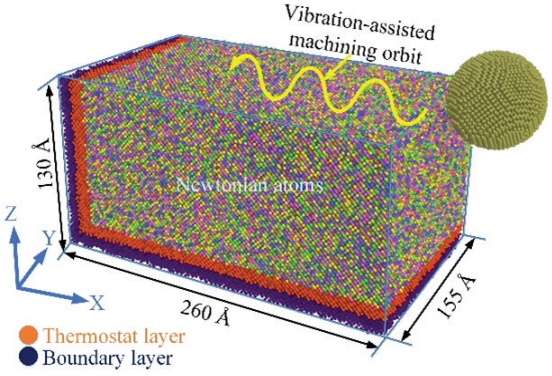

Figure 1. MD simulation model of FeNiCrCoTi subjected to tool vibration during machining.

To study the effect of machining velocity on the vibration-assisted machining behavior of FeNiCrCoTi monocrystal, molecular dynamics (MD) simulations are performed using the Large-scale Atomic/Molecular Massively Parallel Simulator (LAMMPS) [10]. The simulation model is illustrated in Fig. 1. The atoms are divided into three groups: Newtonian layer, thermostat layer, and fixed boundary layer. Periodic boundary conditions are applied along the Y-direction. The machining tool is modeled as a rigid spherical diamond tip with a radius of 30 Å. The system is first relaxed for 80 ps at 300 K to reach equilibrium. During machining, the thermostat group is controlled by the canonical ensemble, while Newtonian atoms evolve under the microcanonical ensemble [11]. The machining is carried out along the X-direction on the (001) surface of the FeNiCrCoTi monocrystal, with a machining depth of 20 Å and machining length of 120 Å. Tool vibration is applied in the Y-direction following a sinusoidal trajectory, expressed as $y(t) = A \cdot \sin(2\pi ft)$, where A and f represent the vibration amplitude and frequency, respectively. In this study, the vibration amplitude is fixed at 15 Å and the vibration frequency at 15.6 GHz, while different machining velocities of 25, 50, 100, and 200 m/s are considered to evaluate their effects. The interatomic interactions are described by the embedded-atom method (EAM) potential for the FeNiCrCoTi alloy, which has been widely validated for multicomponent metallic systems [5, 12]. The Lennard-Jones potential is employed to represent the interaction between the diamond tool and substrate atoms [13]. The LJ potential has been extensively applied in MD simulations of tool–workpiece contact because it captures the short-range repulsive forces when atoms overlap and the weak attractive van der Waals interactions at larger distances. This combination ensures accurate description of both metallic bonding and tool-workpiece contact. The structural evolution and deformation behavior are examined in OVITO, where defect configurations and atomic displacements are characterized through common neighbor analysis (CNA) and the dislocation extraction algorithm (DXA) [14].

3. Results and discussion

The machining velocity is an important factor influencing the vibration-assisted machining process [15]. To investigate the effect of velocity on the machining behavior of HEA, four different velocities of 25, 50, 100, and 200 m/s are applied. The machining process is carried out at a penetration depth of 20 Å, a vibration amplitude of 15 Å, and a vibration frequency of 15.6 GHz. The results of the machining forces, including normal, tangential, lateral, and total components, are presented. Fig. 2 shows the variation of machining forces with machining length at different velocities. The normal and tangential forces increase with machining length for all cases, and their magnitudes become larger as the velocity increases. At low velocity (25 m/s), the forces rise steadily with relatively small fluctuations. When the velocity increases to 100 and 200 m/s, the forces become much higher and show stronger oscillations along the machining path. In the lateral direction, the forces fluctuate around zero, but the amplitude of oscillation changes significantly with velocity. The total machining force follows the same

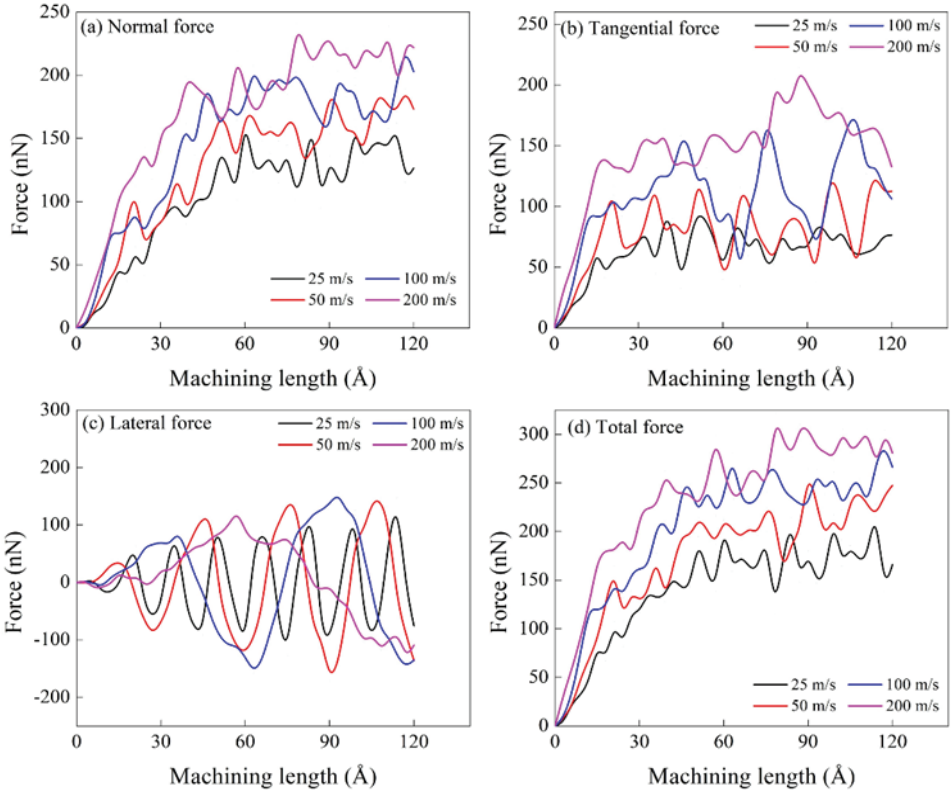

Figure 2. Change of machining force during vibration-assisted machining at different velocities.

trend as the normal and tangential forces, increasing with velocity and machining length. These results suggest that higher machining velocity enhances both the average value and fluctuation of machining forces, which strongly affects the dynamic cutting behavior and material removal process.

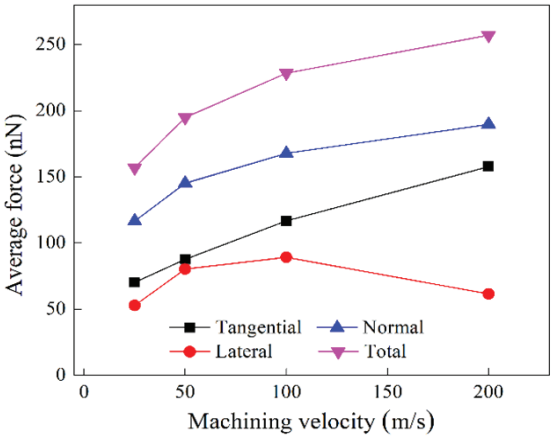

Figure 3. Average machining force during vibration-assisted machining at different velocities.

To compare the force differences in more detail, the force components during the stabilization phase are averaged, and the results are shown in Fig. 3. The normal, tangential, and total forces exhibit a clear increasing trend with velocity. At higher cutting speeds, atoms in the workpiece have less time to relax and rearrange, resulting in insufficient recovery between successive tool interactions. Consequently, larger forces are required to sustain the deformation, which explains the significant growth in both the normal and tangential components as velocity rises from 25 m/s to 200 m/s [15]. The lateral force exhibits a different trend. It increases with velocity up to 100 m/s, but decreases when the velocity reaches 200 m/s. The reduction can be explained that at very high velocity, the vibration cycle is relatively long compared to the cutting time, so the tool direction is less affected by oscillation. Thus, the cutting path undergoes fewer directional changes, leading to a smaller average lateral force at 200 m/s. It should be noted that the lateral force is calculated as the average value of the absolute lateral force during the machining process.

Fig. 4 shows the shear strain distribution in the samples after vibration-assisted machining

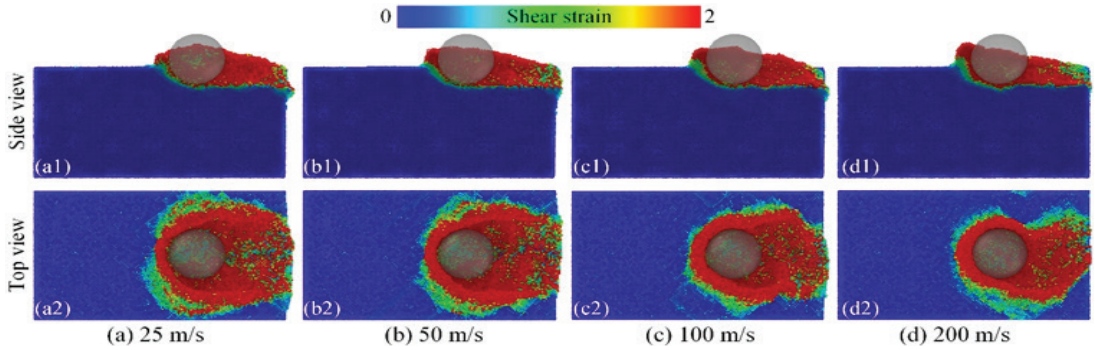

Figure 4. Shear strain distribution in samples after vibration-assisted machining at different velocities.

at different velocities. The high shear strain region appears near the tool tip and in the chip area. However, the extent of shear strain slightly decreases as the machining velocity increases. At low velocity (25 m/s), a broad zone with large shear strain is observed, indicating significant atomic displacement and plastic deformation around the groove. When the velocity increases to 100 and 200 m/s, the high shear strain region becomes narrower and less intense. This reduction can be explained by the fact that at high velocity, atoms have less time to undergo lateral displacement within one vibration cycle, so their shear strain accumulation is limited. Therefore, the tool creates stronger local loads at higher machining velocities, but the reduced relaxation time of the atoms limits their lateral displacement, resulting in a narrower shear strain region.

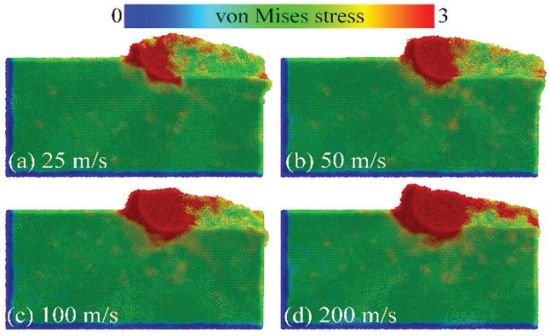

Figure 5. Von Mises stress distribution in samples after vibration-assisted machining at different velocities.

Fig. 5 presents the von Mises stress distribution after machining at different velocities. A high stress concentration appears in front of the tool and inside the chip region, while the surrounding area is relatively uniform. The shear strain patterns in Fig. 4 correlate well with the stress fields shown in Fig. 5. When the machining velocity increases from 25 m/s to 200 m/s, both the size and intensity of the stress region increase significantly. At 200 m/s, the stress distribution is much denser, with a broader high-stress zone compared with lower velocities. This indicates that higher machining velocity causes stronger stress accumulation around the cutting tool, which corresponds well with the increase in machining forces shown earlier.

Fig. 6 shows the temperature distribution in the samples after vibration-assisted machining at different velocities. The elevated stresses at higher velocities contribute to greater plastic work and frictional dissipation, which directly increases the temperature around the tool tip and chip region. As the machining velocity increases from 25 m/s to 200 m/s, the high-temperature zone becomes larger and the peak temperature rises noticeably. At low velocity, only a small area near the groove reaches high temperature, while at 100 and 200 m/s, the heated region extends deeper into the substrate and the chip is almost completely covered by red color. This indicates that higher machining velocity leads to stronger energy dissipation and frictional heating, which enlarges the affected zone.

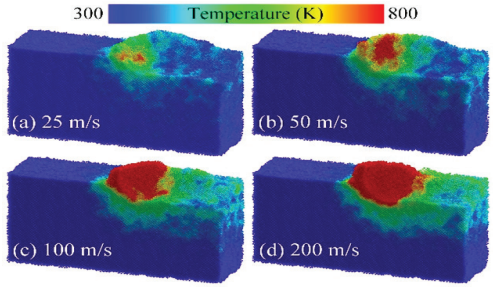

Figure 6. Temperature distribution in samples after machining at different velocities.

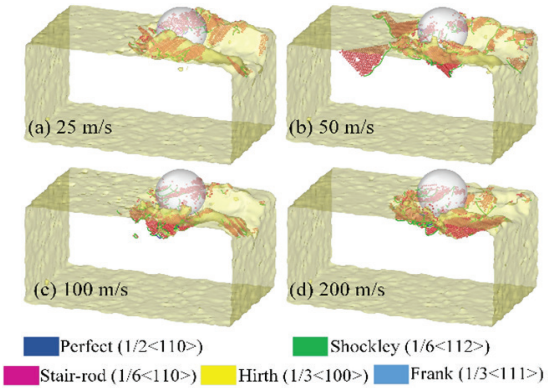

Figure 7. Dislocation distribution in samples after vibration-assisted machining at different velocities.

Fig. 7 shows the dislocation distribution in the samples after vibration-assisted machining at different velocities. Various types of dislocations, such as perfect, Shockley partial, stair-rod, and Hirth, are observed near the cutting tool and in the chip region. Along with the dislocations, red-colored atoms in HCP structure are detected, representing stacking faults formed during the cutting process. At 25 m/s, a dense dislocation network and a large number of stacking faults appear near the tool tip, indicating strong plastic activity. When the velocity increases to 50 and 100 m/s, the dislocation structures extend further along the machining direction, while stacking faults are still visible around the groove. At 200 m/s, both the dislocation density and the number of stacking faults are reduced, suggesting that very high velocity suppresses defect accumulation. These results indicate that Shockley partial dislocations and stacking faults dominate the plastic deformation, while the overall defect activity decreases at excessively high velocity.

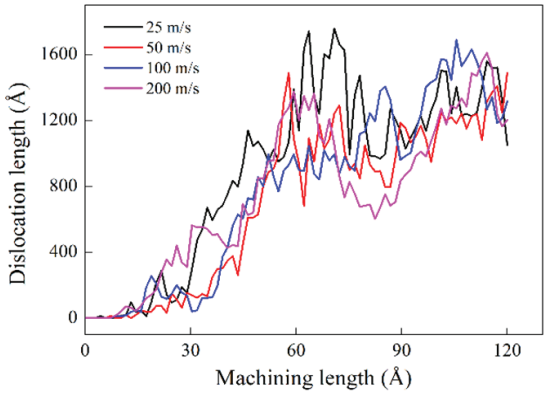

Figure 8. Evolution of dislocation length in samples during vibration-assisted machining at different velocities.

Fig. 8 presents the evolution of dislocation length during machining at different velocities. The dislocation length increases rapidly at the early stage of cutting, and then fluctuates as the machining distance increases. The sample at 25 m/s exhibits the largest dislocation length, reflecting strong dislocation generation and accumulation. For 50 and 100 m/s, the dislocation length still rises but stabilizes at a moderate level with fewer fluctuations. At 200 m/s, the dislocation length is significantly lower, indicating that very high velocity suppresses dislocation activity in the workpiece. This trend agrees with the dislocation distribution results in Fig. 7 and confirms that machining velocity strongly influences the balance between defect formation and stress accumulation.

Fig. 9 compares the surface shapes after vibration-assisted machining at different velocities. The color map indicates the atom height (Z). It can be observed that the samples after machining show a clear groove with similar depth, but the groove at 25 m/s is noticeably wider than at higher speeds. At 25 m/s more atoms are displaced laterally and form larger side protrusions, while at higher velocities the displaced atoms tend to concentrate more in a compact chip in front of the tool and the groove becomes narrower. This pattern suggests that lower speed produces larger lateral material spread, whereas increasing velocity reduces sideways displacement even if the groove depth remains comparable.

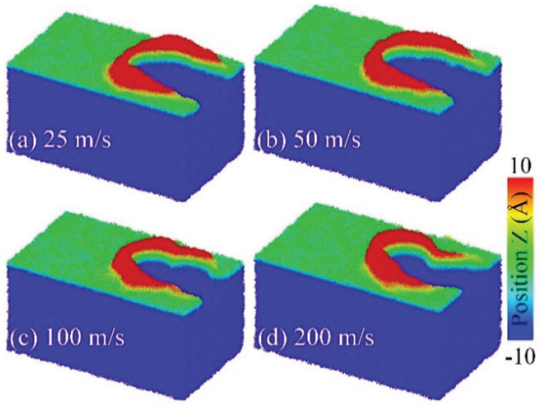

Figure 9. Surface morphology of samples after vibration-assisted machining at different velocities.

Fig. 10 shows the number of worn atoms versus the machining length for each velocity. The number of worn atoms increases steadily with machining

distance, and is highest at 25 m/s throughout the entire process. The curves at 50 m/s and 100 m/s are below 25 m/s, and 200 m/s gives the smallest number of worn atoms. This is consistent with Fig. 9 in that the wider groove and larger edge buildup at 25 m/s correspond to more atoms removed, while the higher velocity reduces the number of atoms removed horizontally and thus reduces the total number of worn atoms.

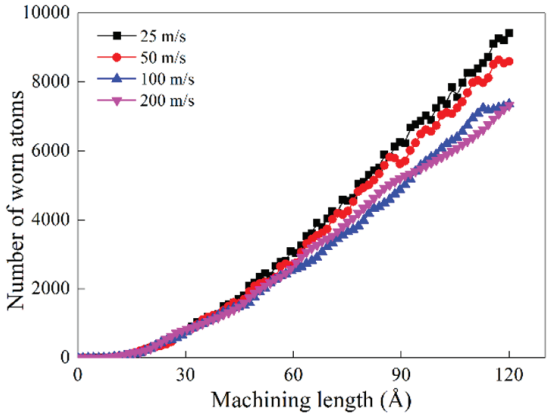

Figure 10. Number of worn atoms of samples during vibration-assisted machining at different velocities.

4. Conclusion

This work examined the effect of machining velocity on vibration-assisted nano-machining of FeNiCrCoTi monocrystal using MD simulation. The results reveal that the normal, tangential, and total forces increase with velocity, while the lateral force decreases at 200 m/s due to reduced tool oscillation. Shear strain around the groove becomes smaller with velocity, indicating limited atomic displacement, whereas von Mises stress rises markedly, reflecting stronger stress accumulation. The temperature distribution also shows a larger high-temperature zone at higher velocities. Defect analysis indicates that at 25 m/s, dislocation networks and stacking faults are dense, and the dislocation length reaches its maximum. At higher velocities, dislocation activity weakens, with the lowest density observed at 200 m/s. Surface morphology results show the groove is widest at 25 m/s, leading to the largest number of worn atoms, while higher velocities produce narrower grooves and fewer removed atoms. These findings provide atomistic insights into the velocity-dependent deformation of HEAs under vibration-assisted machining.

Conflicts of Interest

The authors declare no conflicts of interest.

References

[1] G. Tang et al., "Grain refinement of CoCrFeNiMn high-entropy alloy for improved high-temperature tribological properties," *Journal of Alloys and Compounds,* vol. 1014, p. 178853, 2025.

[2] X. Xu *et al.*, "Cryo-rolling and annealing-mediated phase transformation in Al5Ti2. 5Fe25Cr25Ni42. 5 high-entropy alloy: experimental, phase-field and CALPHAD investigation," *Journal of Materials Science & Technology,* vol. 219, pp. 307-325, 2025.

[3] M. Z. Lin, X. Xiao, C.-H. Xu, W. Lu, Y. Zhang, and W. B. Liao, "A nanostructured TiZrNbTaMo high-entropy alloy thin film with exceptional corrosion properties for biomedical application," *Applied Surface Science,* vol. 684, p. 161859, 2025.

[4] Z. Chen, W. Chen, B. Wu, X. Cao, L. Liu, and Z. Fu, "Effects of Co and Ti on microstructure and mechanical behavior of Al0. 75FeNiCrCo high entropy alloy prepared by mechanical alloying and spark plasma sintering," *Materials Science and Engineering: A,* vol. 648, pp. 217-224, 2015.

[5] A. Liang, D. C. Goodelman, A. M. Hodge, D. Farkas, and P. S. Branicio, "CoFeNiTix and CrFeNiTix high entropy alloy thin films microstructure formation," *Acta Materialia,* vol. 257, p. 119163, 2023.

[6] Z. Yang, L. Zhu, G. Zhang, C. Ni, and B. Lin, "Review of ultrasonic vibration-assisted machining in advanced materials," *International Journal of Machine Tools and Manufacture,* vol. 156, p. 103594, 2020.

[7] M. A. Khan *et al.*, "A review on recent advancements in ultrasonic vibration-assisted machining of difficult-to-machine materials," *International Journal on Interactive Design and Manufacturing (IJIDeM),* pp. 1-36, 2025.

[8] H. Wu *et al.*, "Unveiling the underlying mechanism of ultrasonic vibration assisted machining: Tip-based single asperity nanoscratching experiments and insights from molecular dynamics simulations," *Journal of Manufacturing Processes,* vol. 140, pp. 78-90, 2025.

[9] Q. Wang, J. Guo, W. Chen, and Y. Tian, "Molecular dynamics simulations of tensile properties for FeNiCrCoCu high-entropy alloy," *Materials Today Communications,* vol. 38, p. 108187, 2024.

[10] A. P. Thompson *et al.*, "LAMMPS-a flexible simulation tool for particle-based materials modeling at the atomic, meso, and continuum scales," *Computer physics communications,* vol. 271, p. 108171, 2022.

[11] Z. H. Sun, J. Zhang, G. X. Xin, L. Xie, L. C. Yang, and Q. Peng, "Tensile mechanical properties of CoCrFeNiTiAl high entropy alloy via molecular dynamics simulations," *Intermetallics,* vol. 142, p. 107444, 2022.

[12] M. Yang *et al.*, "Atomistic insights into the effects of Cr content on CoCrxFeNiTi tribological behavior: a molecular dynamics study," *Materials & Design,* p. 114156, 2025.

[13] J. Qiu, Z. Xu, J. Song, C. Hu, L. Miao, and X. He, "Molecular dynamics simulation of a new inhomogeneous concentration distribution model based on frictional behavior of FeNiCrCoCu high-entropy alloy," *Materials Today Communications,* vol. 35, p. 106337, 2023.

[14] A. Stukowski, "Visualization and analysis of atomistic simulation data with OVITO–the Open Visualization Tool," *Modelling and simulation in materials science and engineering,* vol. 18, no. 1, p. 015012, 2009.

[15] J. Xi, X. Ban, W. Ba, Z. Hui, L. Deng, and H. Qiu, "Molecular dynamics simulation of scratching parameters in diamond grit scratching single-crystal silicon carbide," *Materials Science in Semiconductor Processing,* vol. 199, p. 109838, 2025.

CƠ CHẾ BIẾN DẠNG PHỤ THUỘC VẬN TỐC CỦA HỢP KIM ENTROPY CAO FeNiCrCoTi TRONG QUÁ TRÌNH GIA CÔNG HỖ TRỢ RUNG ĐỘNG

Tóm tắt:

Gia công hỗ trợ rung động đã cho thấy tiềm năng lớn trong việc cải thiện khả năng gia công các vật liệu cứng và giòn, tuy nhiên cơ chế của nó đối với hợp kim entropy cao (HEA) vẫn chưa được làm sáng tỏ. Trong nghiên cứu này, các mô phỏng động lực học phân tử được sử dụng để khảo sát hành vi phụ thuộc vận tốc của đơn tinh thể FeNiCrCoTi trong quá trình gia công nano có hỗ trợ rung động. Phân tích tập trung vào lực cắt, biến dạng trượt, ứng suất von Mises, sự tiến triển của lệch mạng, phân bố nhiệt độ và hình thái bề mặt. Kết quả cho thấy khi vận tốc tăng, lực pháp tuyến và tiếp tuyến, sự tập trung ứng suất và nhiệt độ cục bộ đều tăng lên, trong khi biến dạng trượt, sự tích lũy lệch mạng, chiều rộng rãnh và số nguyên tử bị mài mòn lại giảm. Những phát hiện này cung cấp các hiểu biết mới ở cấp độ nguyên tử về cơ chế biến dạng và loại bỏ vật liệu của HEA trong gia công hỗ trợ rung động.

Từ khóa: *Gia công hỗ trợ rung động, Mô phỏng động lực học phân tử, Vận tốc, Hợp kim entropy cao.*